
Building spatial world models from sparse transitional episodic memories

Zizhan He^{1,3} Maxime Daigle^{2,3} Pouya Bashivan^{1,2,3}

¹ Department of Computer Science, McGill University

² Department of Physiology, McGill University

³ Mila, Université de Montréal

Abstract

Many animals possess a remarkable capacity to rapidly construct flexible mental models of their environments. These world models are crucial for ethologically relevant behaviors such as navigation, exploration, and planning. The ability to form episodic memories and make inferences based on these sparse experiences is believed to underpin the efficiency and adaptability of these models in the brain. Here, we ask: Can a neural network learn to construct a spatial model of its surroundings from sparse and disjoint episodic memories? We formulate the problem in a simulated world and propose a novel framework, the Episodic Spatial World Model (ESWM), as a potential answer. We show that ESWM is highly sample-efficient, requiring minimal observations to construct a robust representation of the environment. It is also inherently adaptive, allowing for rapid updates when the environment changes. In addition, we demonstrate that ESWM readily enables near-optimal strategies for exploring novel environments and navigating between arbitrary points, all without the need for additional training.

1 Introduction

When visiting a new city, we quickly piece together scattered memories—an alley passed on a walk, a glimpse of a landmark from a taxi—into a mental map that lets us navigate, explore, and plan. This ability to build a coherent model of the world from fragmented experiences, and to use it flexibly for imagining new routes or outcomes, is a core feature of human intelligence that is fundamental to planning, problem-solving, and decision-making, all of which are crucial for survival (4).

How do humans achieve this extraordinary feat? Insights from neuroscience and psychology provide compelling evidence for the neural mechanisms underpinning this capacity. One pivotal discovery is the dual role of a key brain area called the medial temporal lobe (MTL) in both spatial representations and episodic memories. Individual neurons within the MTL exhibit spatial selectivity, firing in response to specific locations (39; 23), while collectively forming a population code that represents an animal’s instantaneous position in space (59). In parallel, MTL plays a critical role in the formation of episodic memories, enabling the rapid acquisition of associations between arbitrary stimuli (27). Strikingly, lesions to this area result in profound deficits: individuals lose not only their ability to explore and navigate effectively (32) but also their capacity to form episodic memories (45) and imagine novel scenarios (25). These converging findings strongly suggest that the MTL constructs structured relational networks, integrating overlapping episodic memories into a cohesive framework (12; 35). This mechanism may underlie a flexible and adaptive world model, allowing for inferences about spatial relationships beyond immediate perception.

Despite these insights, most prior computational approaches to world modeling have relied on learning from continuous sequences of recent observations and actions (19; 20; 54; 34), fixed hand-designed circuitry for representing and updating spatial information (52; 5; 33), allocentric observations

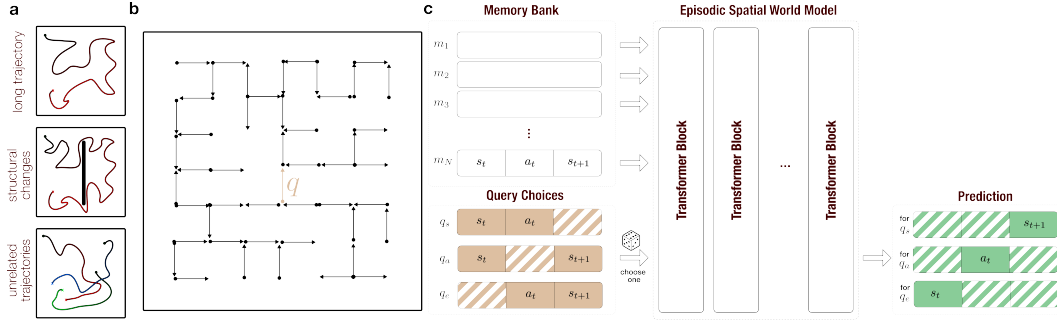


Figure 1: **Episodic Spatial World Model.** **a)** Three common scenarios that hinder the ability of typical world models to generalize effectively. (top) Observation of the full environment may take many time steps leading to long sequences; (middle) Specific parts of the environment may be changed dynamically; (bottom) Information about a particular environment may be collected across separate exposures to the environment and not within a single one. **b)** . Memory bank and query selection in a square grid environment. **c)** Architecture of ESWM and training procedure. Model input consists of a bank of transitional memories (corresponding to the black arrows in (b)) and a single query (q arrow in (b)), with either start-state, action, or end-state randomly masked with equal chances. The sequence of transitions is processed by a sequence model (e.g, Transformer encoder block) and the model parameters are updated to output the correct value for the masked component.

(30), and iterative update procedures that hinders their ability to quickly adapt to environmental changes(52; 5; 47). These models are typically trained on large datasets collected from a given environment, with knowledge encoded in their weights. While effective in certain contexts, such approaches face inherent limitations. For instance, agents may encounter different parts of an environment at widely separated times, visit states along arbitrary and unrelated trajectories that do not form continuous sequences, or experience environments that undergo structural changes (Fig.1a). These challenges hinder the ability of sequence-based models to generalize effectively in environments where observations are disjoint and episodic.

This raises a key question: Can a neural network rapidly construct a coherent spatial map of the environment using only sparse and disjoint episodic memories? Drawing inspiration from the neuroscience of memory and navigation, we introduce the Episodic Spatial World Model (ESWM), a framework designed to infer spatial structure from independently acquired episodic experiences. While in conventional world-model training, a network’s weights encode the full dynamics of a single environment via long, continuous trajectories, ESWM meta-trains the model to predict unseen transitions from a minimal set of one-step transitions sampled across diverse environments. This approach allows the model to infer missing information, connect distant experiences, and dynamically adapt to structural changes.

Our main contributions are as follows:

1. We introduce ESWM, a framework for modeling spatial environments from a minimal set of previously experienced episodic transitions in each environment.
2. We demonstrate that the ESWM’s latent space organizes into a geometric map that closely reflects the spatial structure of the environment.
3. By studying the behavior of the model across various scenarios, we show that ESWM’s latent structure dynamically updates in response to changes in its memories, enabling it to incorporate previously unseen regions and adapt to structural modifications, such as the addition of obstacles.
4. We demonstrate that the learned world model enables near-optimal exploration of novel environments and facilitates navigation between arbitrary points within those environments—all without requiring additional training.

2 Related Works

2.1 World models

Humans excel at forming abstract representations of spatial and temporal information from egocentric observations and action, enabling efficient interaction with complex, dynamic environments. Inspired by this cognitive ability, prior work in artificial intelligence, particularly in reinforcement learning (RL) (48), has explored world models to improve sample efficiency and planning effectiveness (22; 44; 50). World models provide agents with a predictive understanding of their environment by modeling past and present states and forecasting future outcomes (19). In spatial settings, agents have been trained to predict future sensory observations following arbitrary actions (47; 54; 34) while in vision, methods such as image reconstruction (53; 1) and video prediction (28; 18) enable simulation of future frames or latent dynamics. These approaches have demonstrated success in domains such as video games (21; 44; 28) and robotic control tasks (18; 11).

More recently, the emergence of transformer architectures (51) has opened new possibilities for improving world models. Recent works such as TWM (43), STORM (61), and IRIS (36) have leveraged transformers-based world models to improve performance on sample-limited benchmarks like Atari 100k. However, unlike our proposed model, these models train extensively on a single environment and absorb the knowledge about that environment in the model’s weight.

2.2 Navigation Agents

The concept of a spatial or cognitive map (40) has been thought to enable navigation and spatial reasoning. This spatial map, an internal neural representation of an environment, encodes landmarks, resources, and shelters, enabling organisms to plan and navigate (39; 13; 56). Several studies have demonstrated that similar spatial representations emerge in neural networks trained on navigation tasks (16). For example, Banino et al. (2) and Cueva and Wei (10) showed that spatial representations arise in recurrent neural networks trained for path integration, aiding navigation through implicit spatial reasoning. In parallel, neural networks lacking explicit mapping modules have achieved high performance on navigation tasks, demonstrating that general-purpose architectures can achieve high navigation accuracy in novel environments (57; 41; 31; 46). For instance, Reed et al. (41) showed that a general-purpose transformer model could perform a wide range of embodied tasks, including navigation.

Neuroscience findings suggest that the brain employs common cognitive mapping strategies across both spatial and non-spatial domains, potentially encoding abstract information like semantic content within these maps (3). For instance, this perspective frames reasoning as a form of navigation through a cognitive map of concepts, relationships, and logical rules. Wijmans et al. (58) recently showed that spatial representations can emerge in navigation-agnostic neural network architectures trained for navigation, emphasizing memory’s role in shaping these spatial representations. This raises a key question: *Can spatial maps also emerge in general-purpose models not explicitly trained for navigation?*

3 Methods

3.1 Episodic Spatial World Model

We define an episodic memory as a one-step transition in a spatial environment, represented by the tuple (s_s, a, s_e) —denoting the source state, action, and end state, respectively. A memory bank M for a given environment is an unordered set of such transitions, constructed to be: *Disjoint*, transitions do not form a continuous trajectory; *Spanning*, the transitions collectively form a connected graph covering all locations; *Minimal*, removing any transition would disconnect the graph (Fig. 1b). We algorithmically generate such memory banks to sparsely cover each environment (Extended Methods A.3). Importantly, a single room may yield multiple valid memory banks, enabling our meta-training setup.

We formulate spatial modeling as the ability to infer any missing component of an unseen but plausible transition q —that is, a query transition not present in M (Fig.1b). The task is to predict the masked element (either s_s , a , or s_e) of q , given the other two and the memory bank M (Fig.1c).

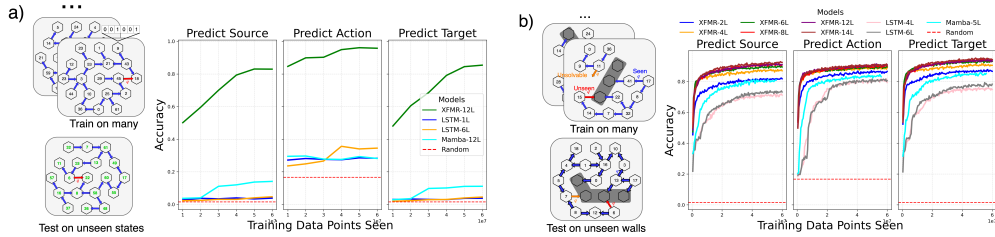


Figure 2: **Evaluation accuracy in a) Open Arena and b) Random Wall.** In both schematics, blue arrows are transitions in the memory bank and the q -labeled arrows are examples of query transitions $q = (s_s, a, s_e)$. In Open Arena, the states are represented as 6-bit binaries and the model is tested in environments entirely filled with unseen states, while in Random Wall, the states are integers and the model is tested on its generalizability to unseen wall patterns. In addition, a random subregion is masked in Random Wall and the query q can be either unsolvable, unseen, or seen, depicted as q -labeled arrows with different colors. The Random Wall displayed here is a scaled down version of what the model is trained on (19 locations versus 36 locations). XFMR is short for Transformer.

Formally, our Episodic Spatial World Model (ESWM) is a function f that takes as input a memory bank M and a partially masked transition q , and predicts the complete transition q^* :

$$q^* = f(M, q) \quad (1)$$

To train ESWM, we adopt a meta-learning approach where on each trial (i.e. sample), we randomly sample: (1) An environment e ; (2) A disjoint memory bank M from e ; (3) A plausible query transition q from $(e \setminus M)$; (4) A masking choice (randomly masking s_s , a , or s_e). This process ensures that the model must reason over episodic structure rather than memorize specific environments. Notably, our environments (Open Arena, Random Wall; detailed below) contain up to 10^{33} and 5×10^{36} possible configurations, respectively—making memorization intractable (Extended Methods A.2, Fig. 2).

3.2 Model Selection and Training

We considered three neural network architectures for f , 1) Encoder-only transformer with no positional encoding(51), 2) long short-term memory (LSTM) (26), and Mamba (17). To create an embedding of each transition (s_s, a, s_e) , each component of the transition (i.e. source state, action, and end state) are projected onto the same dimensional space using separate linear projections. The three projected values are averaged to produce a single embedding of the transition.

Each model receives as input the concatenated sequence of randomly-permuted memory bank embeddings and query embeddings, treating each embedding (i.e. each transition) as a distinct input token (Fig.1b). The LSTM and Mamba model receives a sequence of tokens that start with M and end with the query token. Three separate linear heads read out the model’s prediction on the three parts $(s_s, a, s_e)_q$ from the final layer’s last token. We use cross-entropy loss between predicted and actual states and actions. Equal weight is assigned to each prediction (s_s, a, s_e) . Training is done over 460k iterations with a batch size of 128 and a cosine learning rate schedule.

3.3 Model Evaluation

We evaluate ESWM in a family of discrete, hexagonally structured grid environments. The hexagonal layout allows for six possible actions per location, offering richer connectivity than traditional square grids. Each location in the environment is assigned an integer-valued observation, drawn from a predefined set of states. An environment is uniquely defined by its mapping from states to spatial locations, allowing us to generate a vast number of distinct rooms by randomly shuffling this mapping—critical for our meta-learning objective (Extended Methods A.2).

We design two types of environments to test generalization: (1) Open Arena to evaluate generalization to unseen observations and; (2) Random Wall to evaluate generalization to unseen structures.

Open Arena: Each room consists of 19 locations and 64 possible state values. These states are represented compositionally as 6 binary bits (Fig. 2a). For action prediction, the model performs 6-way classification (one for each action). For source and end state prediction, the task is broken into six independent binary classification problems—one for each bit. To test generalization, we ensure that *training and testing states are mutually exclusive*: the model is never exposed to the same state values during training and testing. This forces it to build representations that support spatial reasoning even in environments filled with previously unseen but compositionally generated state observations.

Random Wall: In this setting, rooms are larger (36 locations) and contain 36 possible states, each represented as a unique integer. The association between locations and states is still randomized for each sample. Importantly, each room also includes a randomly shaped wall composed of obstacles that block movement (i.e., attempting to enter a wall cell returns the agent to its original location) (Fig. 2b). The model must generalize to unseen state-location associations and wall configurations during testing. Prediction tasks mirror the Open Arena setting: 6-way classification for actions, and 36-way classification for source and end states.

We also allow the model to output “*I don’t know*” (implemented as an additional classification category) when the prediction is not possible given the available memory bank. To simulate such scenarios, we occasionally create trials in which some of the memories covering a part of the environment are removed from the memory bank and query the model with a transition that crosses between known and unknown regions (“unsolvable queries”). This enables the model to identify uncertainty and encourages adaptive exploration in novel, obstacle-rich environments. During training, query transitions are sampled with the following probabilities: 68% unseen (plausible but not in the memory bank), 17% seen (present in the memory bank), 15% unsolvable (crossing into unknown regions) (Appendix A.4).

4 Results

4.1 Simulating Spatial Environments

We first assessed ESWM on its core ability to predict missing elements of unseen transitions given a set of memories from an environment and a partially observable query. We found a stark difference between the model types in Open Arena setting (Fig.2a). The transformer model excelled at learning this task, reaching accuracies of 82.9%, 95.8%, and 85.4% on source state, action, and end state prediction tasks respectively. In contrast, LSTM and Mamba models struggled to reach above chance on this task for both training and testing. This suggests that the attention mechanism in Transformer architectures—reminiscent of classic content-addressable memory models (29)—plays a key role in learning generalizable world models from episodic memories. However, a closely related approach by Coda-Forno et al. (8), which relies on a key-value memory table and hand-engineered K-nearest neighbor lookup, fails to predict unseen queries (Fig. A8). This highlights the importance of using learnable, deep attention-based mechanisms for flexible inference.

In the second scenario, the Random Wall, we found that all models were capable of learning the task (Fig.2b). Although, there was a substantial gap between transformer-based models and other models, even with equal number of parameters (LSTM-4L, Transformer-2L, and Mamba-5L). This showed that ESWM learned a general strategy for modeling an environment from sparse and disjoint episodic memories of transitions within that environment that it could then generalize to any environment with different structures.

4.2 Spatial Maps Emerge Robustly From the Latent Space

To simulate an unseen transition, ESWM must integrate disjoint memory fragments into a coherent internal map that reflects both observed states and obstacles. Inspired by low-dimensional, environment-like neural manifolds in rodents’ MTL (38), we applied ISOMAP (49) (Extended Methods A.5) to ESWM’s latent space. The resulting manifolds revealed that ESWM consistently organizes its internal representations to mirror the spatial layout of each specific environment.

In obstacle-free environments, the manifold adopts a smooth, saddle-like shape (Fig.3a). When obstacles are introduced, they create localized discontinuities that correspond precisely to blocked regions in physical space (Fig.3b). This structure is remarkably robust and persists under out-of-distribution obstacle shapes (Fig. A1, A2), partial observation of environments (Fig. A3), across

architectures (LSTM, Transformer, Mamba; Figs.A1–A2), and throughout all transformer layers, which become progressively more continuous with depth (Fig.A5). All prediction tasks (start-state, action, end-state) yield similar maps (Fig.A3a). Quantitatively, path lengths in latent and physical spaces correlate strongly ($R^2 = 0.89$, $N_{\text{path}} = 1500$, $N_{\text{env}} = 75$; Fig.A7b), and a linear classifier on ESWM activations can accurately discriminate which of two states is farther from a reference state with $93.42 \pm 0.006\%$ accuracy (chance = 50%, $N_{\text{seed}} = 10$; Extended Methods A.6).

Notably, such structured spatial representation do not emerge in episodic agents trained for navigation, such as Episodic Planning Network (EPN; (42)), despite being trained with meta-RL on the same environments and data as ESWM (Fig.A1, A2; Appendix D).

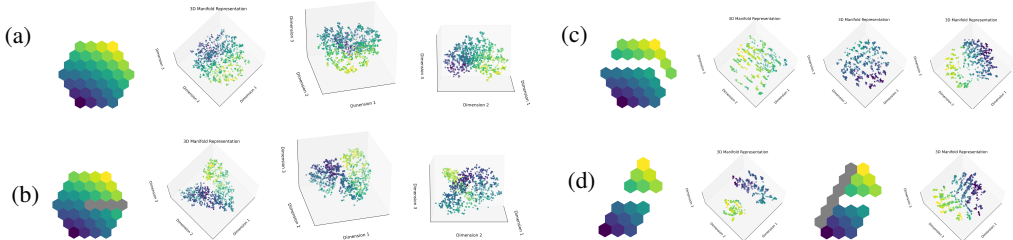


Figure 3: **Spatial map emerges in ESWM’s latent space.** **a), b)** ISOMAP projections of the 2-layer transformer model’s first layer’s activations for action prediction. Different columns are the same projection from different viewing angles. **a)** Spatial map in the absence of obstacles and **b)** in the presence of obstacles (a straight wall). **c), d)** ISOMAP projections of the 14-layer transformer model’s seventh layer’s activations. **c)** From left to right: A sample room with two disjoint regions whose shapes match boundaries’ shape; ESWM’s latent space when a memory bank observing either the top or bottom region is given as input; ESWM’s latent space when a memory bank observing both regions is given as input. **d)** From left to right: A sample room containing two disjoint regions whose shapes give no cues about their relative position; ESWM’s latent space when a memory bank of the room is given as input; Updated room with a new wall, the regions remain disjoint; ESWM’s latent space when a memory bank of the updated room is given as input. See Fig.A1, A2, A3, A4, A5 for more examples.

4.3 Handling Disjoint Memory Clusters

During Random Wall training, memory banks can contain disjoint memory clusters, with no paths between observations in distinct clusters. This leads to uncertainty in spatial relationships as path integration provides no avail. In rare cases, the model is asked to solve queries that bridge disconnected clusters. This raises two questions: (1) Does the model infer the relative positions of disjoint memory clusters (e.g., which part of the room each cluster maps onto)? (2) Which cues enable these inferences?

4.3.1 Inference from Environmental Structure

We observe that when memory clusters are disjoint, the model leverages the underlying structure of the room to infer their relative positions. For example, the model aligns memory clusters with the room’s boundary when their shape matches. This allows the model to piece together disjoint memory clusters, like solving a puzzle, by identifying the configuration that satisfies the invariant structural constraints. Evidence for this behaviour is twofold. First, in the model’s latent space, the disjoint clusters are stitched together, rather than overlapping or disconnecting, to form a smooth surface reflecting the room’s structure (Fig. 3c). Second, the model’s end state prediction distributions, starting from the boundary states of one cluster, are biased towards the boundary states of the inferred neighbouring cluster, instead of exclusively outputting the “I don’t know” option.

4.3.2 Generalization from Observations of Obstacles

In cases where disjoint memory clusters’ shapes do not provide clear cues about their relative locations, the model relies on observations of obstacles to deduce their positions. For instance, given two disjoint clusters of memories, the model initially maps them to different locations in its latent space and outputs predictions exclusively reflecting uncertainty (“I don’t know”). However,

if both clusters observe obstacles, even though the clusters remain disjoint, the model applies its knowledge of common wall shapes (e.g, walls are usually straight) to make inferences about the relative locations of the clusters. In the latent space, the two previously disconnected clusters are connected and aligned along the inferred wall shape to form a continuous representation (Fig. 3d, A4). The model’s predictions are also biased towards the inferred neighbours. Moreover, a single observation of obstacles from both clusters is sufficient for the model to infer the shape of the wall, and therefore infer the relative positions of the clusters (Fig. A4). These results demonstrate that ESWM can leverage the invariant structure of the room and combine observations of obstacles with prior knowledge of wall shapes to construct a coherent spatial representation.

4.4 ESWM Integrates Overlapping Memories

How does ESWM construct its internal spatial map? We find that ESWM’s prediction uncertainty—measured by entropy—increases with the length of the integration path needed to solve a query. That is, when ESWM must stitch together more episodic memories via overlapping states, uncertainty rises (Fig.4a). Introducing shortcut memories that reduce this path length significantly alters the prediction distribution (independent two-sample t-test; $n = 5000, p < 0.001$; Fig.4b). These results suggest that ESWM builds coherent spatial representations by integrating overlapping episodes. Consistent with this, performance improves with denser memory banks, even though they are out-of-distribution (Fig. 4c).

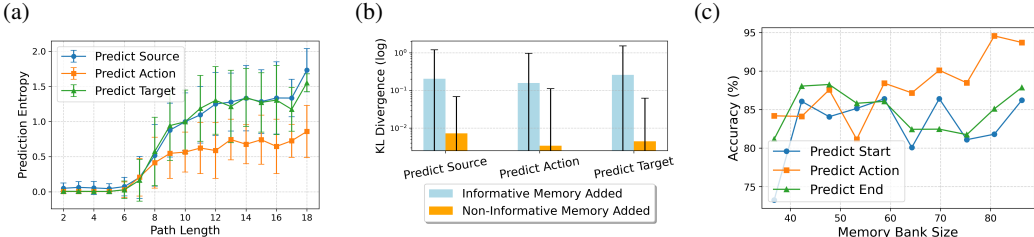


Figure 4: **ESWM integrates memories.** **a)** X-axis represents the shortest path length between the source and end states in the query, with edges corresponding to episodic memories in the memory bank, and the Y-axis is the entropy of ESWM’s prediction probabilities ($n=5000$). **b)** KL divergence between ESWM prediction distributions before and after adding an episodic memory to the memory bank. An informative episodic memory shortens the integration path required for the model to solve the prediction task, while a non-informative episodic memory does not alter the shortest integration path ($n=5000$). **c)** Prediction accuracies for unseen transitions as ESWM receive larger, out-of-distribution, memory banks ($n=2000$). Transformer -14L is used for a) and b) while 4L is used for c).

4.5 Exploration in Novel Environments

So far, we have assumed that ESWM has access to informative episodic memories. However, animals actively acquire such memories through exploration. The ability to rapidly map out novel environments—identifying obstacles, rewards, and threats without prior knowledge—is critical for survival. We show that ESWM enables autonomous exploration in unfamiliar spaces without any additional training.

We designed a simple exploration algorithm based on ESWM’s “I don’t know” predictions (Alg.2). Starting with an empty memory bank, the agent evaluates all possible actions at each step by querying ESWM. It selects the action with the highest predicted uncertainty (i.e., highest “I don’t know” probability) and adds the resulting transition to memory. When ESWM is confident about all immediate actions, the agent performs multi-step lookahead by unrolling the model to identify frontier states with low prediction confidence (60). A prediction is deemed unconfident if ESWM either outputs “I don’t know” or assigns $\leq 80\%$ probability to the predicted outcome.

Interestingly, the agent adopts an efficient zig-zag exploration strategy, only revisiting states when separated by long paths. In the Random Wall environment, ESWM explores 16.8% more unique states than EPN (one-way ANOVA; $n = 1000, F = 2803.63, p < 0.05$; Tukey’s HSD post hoc test: $ESWM > EPN, p < 10^{-3}$), and achieves 96.48% of the performance of an oracle agent with full obstacle knowledge (Fig. A6). When exploration continues until memory is saturated, ESWM

visits on average 90% of all unique states. Moreover, the collected memory banks allow ESWM to predict transitions with 96.71% of the accuracy of those achieved using procedurally generated memory banks. Together, these results highlight ESWM’s ability to support data-efficient, near-oracle exploration and mapping in novel environments.

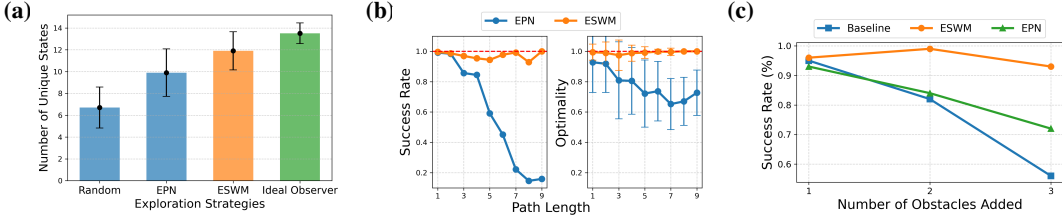


Figure 5: **Exploration, navigation, and adaptability.** **a)** Comparison of exploration strategies based on the number of unique states visited over 15 time steps in Random Wall. The optimal agent explores along the path found by the Traveling Salesman Algorithm over known free space. $N=1000$. **b)** Comparison of navigation success rate and path optimality over path lengths between EPN and ESWM, $n=2400$. **c)** Comparison of navigation success rates with increasing number of unexpected obstacles. The baseline agent is trained on the original environment and tested after structural changes, while ESWM navigates with memory banks from the original environment and needs to autonomously adapt to changes ($n=100$). Random Wall Experiments include 19 locations.

4.6 Navigating with Minimal Spanning Episodic Memories

Internal world models offer the ability to simulate long trajectories — imagining sequences of actions and observations beyond immediate sensory input— towards a certain goal before executing them. We demonstrate that memory-bank-equipped ESWM can be used for such long trajectory planning in obstacle-rich Random Wall. We frame the planning problem as follows: Given a memory bank of an environment and a list of possible actions, an agent must find a sequence of actions to go from any source state S_{source} to any goal state S_{goal} . The agent operates without global information, such as its current location, the positions of obstacles, or the coordinates of the goal. Instead, it relies solely on its current (egocentric) observation, goal state, and fragmented spanning episodic experiences.

4.6.1 Planning by Imagination

We devise a simple strategy relying on ESWM’s ability to infer the end state of any transition given a memory bank, the source state, and the action. Initialized at a state, an agent can imagine multiple steps into the future by querying ESWM on the consequences of all applicable actions, bootstrapping on ESWM’s own predicted end states, and tracking visited states until the goal state is reached (Alg.1). Then the agent can act out the imagined sequence of actions in reality. This can be viewed as Dijkstra’s algorithm applied to a graph whose dynamics can be retrieved through ESWM.

Using this strategy, an ESWM-based navigational agent can navigate between arbitrary states in Random Wall with 96.8% success rate and 99.2% path optimality, outperforming EPN (42) by 18% and 21% respectively (Fig.5b) (one-sided independent t-test; $n=2400$: $ESWM > EPN$ on optimality; $p < 10^{-3}$). Navigation is successful if the agent reaches the target within 15 time steps, and path optimality is defined as the ratio between the shortest and actual path length.

4.6.2 Planning by Guided Imagination

While the previous strategy enables planning, it uniformly searches through the space, unbiasedly imagining the consequences of all actions, even if some move further from the goal. In contrast, animals with internal maps encoding geometric constraints plan biasedly, prioritizing actions that shorten the geodesic distance (i.e., the shortest path length) to the goal. We show that the spatial maps in ESWM’s latent space, which accurately encode obstacles and geodesic distance between states (Fig.A7b), can be used for guided imagination towards the goal.

The previous strategy is akin to Dijkstra’s algorithm, or A* with a null heuristic function (24; 15). The key to efficient planning, which prunes undesirable actions early, then, is a heuristic function containing rich information on the geodesic distances between states in the environment. Inspired by

ISOMAP (49), we construct such a heuristic function h_{latent} as follows (See Alg.4 for pseudocode): 1) Query the model to solve the end state prediction task for all possible (s, a) pairs, collecting activations. 2) Construct a graph G_{latent} where nodes are activations and edges connect nodes within radius R_{latent} (Appendix C). Edges are weighted by the cosine distance between their two endpoints (Fig.A7b). Intuitively, each node on G_{latent} is the activation of predicting the outcome of action a starting at state s . 3) Compute pairwise shortest paths on this graph to create a geodesic distance table h_{latent} .

h_{latent} captures ESWM’s latent spatial map into a look-up table containing information on which action takes you closer to the goal state at every step of imagination. A* guided imagination with h_{latent} , improves planning efficiency by 57% (Fig.A7a), as measured by the number of states visited, over Dijkstra’s while maintaining path optimality (Fig.A7c). Furthermore, greedy policy based on h_{latent} achieves 70% success in navigating around obstacles (Fig.A7a). These results suggest that structured latent spaces in world models can serve as efficient heuristics for planning.

4.7 ESWM Enables Fast Adaptation to Changes

Unlike traditional world models that embed environment knowledge in their weights, ESWM decouples memory from reasoning. This separation makes ESWM inherently adaptable to changes: when the environment changes, no retraining is needed—only the external memory bank is updated. Because ESWM operates on sparse, one-step transitions, targeted edits to memory are straightforward. We demonstrate this flexibility in a dynamic navigation task. After introducing substantial changes—such as new obstacles—an ESWM agent continues to navigate between arbitrary states with a 93% success rate (Fig.5c).

The adaptive agent works as follows: Given a (possibly outdated) memory bank M , it plans a path from s_{start} to s_{goal} (Section 4.6). During execution, it compares predicted observations with actual ones. When mismatches occur (indicating environmental changes), the agent removes outdated transitions (where s_s or s_e match the predicted observation from M), prompting exploration (Section 4.5) to fill the gaps. After acquiring new transitions, the agent replans with the updated memory.

Compared to a baseline LSTM agent trained via RL to navigate between any two states in a fixed environment (Extended Method A.7) and EPN (see Section D), ESWM is far more robust to change. For example, after adding a new wall consisting of multiple contiguous obstacles, ESWM maintains a 93% navigation success rate, whereas EPN and the baseline drop to 72% and 56% respectively (see Fig.5c). Unsurprisingly, the baseline agent fails to form any structured latent spatial map.

5 Discussion

In this work, we introduced ESWM, a neural network model that can rapidly construct a coherent spatial world model from sparse and fragmented one-step transitions. ESWM exhibits strong spatial reasoning and supports downstream tasks like exploration and navigation—even without explicit training for them. Unlike prior models that rely on fixed circuitry for spatial representation (52; 5; 33), ESWM learns both representation and update mechanisms directly from experience. It encodes new memories in a single shot, avoiding the iterative parameter tuning required by earlier approaches (52; 5; 47). By storing transitional memories instead of state-observation pairs (54; 9; 55), ESWM also adapts quickly to environmental changes, such as the addition or removal of obstacles—an area where many existing models struggle.

While our focus was on a grid environment where episodic memories are transitions between integer observations via allocentric actions (e.g, 'go north'), preliminary results on MiniGrid (6) (Fig.A9) show that ESWM’s prediction performance and internal map representation generalize to a more complex setting with pixel observations and egocentric actions (e.g, 'turn left'). Yet still, such formulation of episodic memories greatly simplifies the complex sensory observations and egocentric motion cues typically associated with humans’ — a gap we leave for future work. Another limitation is the use of highly controllable and simplified environments, which allowed us to scale up the training and control different aspects of the environment and data freely. Future work could explore extending this approach to more realistic settings with natural, complex sensory information. Although theoretical, our work has potential societal impacts in autonomous navigation and exploration, highlighting the need for safe, ethical, and responsible deployment (see Section E).

References

- [1] Eloi Alonso, Adam Jelley, Vincent Micheli, Anssi Kanervisto, Amos Storkey, Tim Pearce, and François Fleuret. Diffusion for world modeling: Visual details matter in atari. *arXiv preprint arXiv:2405.12399*, 2024.
- [2] Andrea Banino, Caswell Barry, Benigno Uribe, Charles Blundell, Timothy Lillicrap, Piotr Mirowski, Alexander Pritzel, Martin J Chadwick, Thomas Degris, Joseph Modayil, et al. Vector-based navigation using grid-like representations in artificial agents. *Nature*, 557(7705):429–433, 2018.
- [3] Timothy EJ Behrens, Timothy H Muller, James CR Whittington, Shirley Mark, Alon B Baram, Kimberly L Stachenfeld, and Zeb Kurth-Nelson. What is a cognitive map? organizing knowledge for flexible behavior. *Neuron*, 100(2):490–509, 2018.
- [4] Max Bennett. *A brief history of intelligence: evolution, AI, and the five breakthroughs that made our brains*. HarperCollins, 2023.
- [5] Sarthak Chandra, Sugandha Sharma, Rishidev Chaudhuri, and Ila Fiete. Episodic and associative memory from spatial scaffolds in the hippocampus. *Nature*, 638(8051):739–751, February 2025. ISSN 1476-4687. doi: 10.1038/s41586-024-08392-y. URL <https://www.nature.com/articles/s41586-024-08392-y>. Publisher: Nature Publishing Group.
- [6] Maxime Chevalier-Boisvert, Bolun Dai, Mark Towers, Rodrigo Perez-Vicente, Lucas Willems, Salem Lahlou, Suman Pal, Pablo Samuel Castro, and Jordan Terry. Minigrad & mineworld: Modular & customizable reinforcement learning environments for goal-oriented tasks. In *Advances in Neural Information Processing Systems 36, New Orleans, LA, USA*, December 2023.
- [7] Kyunghyun Cho, Bart van Merriënboer, Caglar Gulcehre, Dzmitry Bahdanau, Fethi Bougares, Holger Schwenk, and Yoshua Bengio. Learning phrase representations using rnn encoder-decoder for statistical machine translation, 2014. URL <https://arxiv.org/abs/1406.1078>.
- [8] Julian Coda-Forno, Changmin Yu, Qinghai Guo, Zafeirios Fountas, and Neil Burgess. Leveraging Episodic Memory to Improve World Models for Reinforcement Learning. https://memari-workshop.github.io/papers/paper_3.pdf, 2022. [Accessed 09-05-2025].
- [9] Julian Coda-Forno, Changmin Yu, Qinghai Guo, Zafeirios Fountas, and Neil Burgess. Leveraging Episodic Memory to Improve World Models for Reinforcement Learning. *NeurIPS MemARI Workshop*, 2022.
- [10] Christopher J Cueva and Xue-Xin Wei. Emergence of grid-like representations by training recurrent neural networks to perform spatial localization. *arXiv preprint arXiv:1803.07770*, 2018.
- [11] Frederik Ebert, Chelsea Finn, Sudeep Dasari, Annie Xie, Alex Lee, and Sergey Levine. Visual foresight: Model-based deep reinforcement learning for vision-based robotic control. *arXiv preprint arXiv:1812.00568*, 2018.
- [12] Howard Eichenbaum. Hippocampus: Cognitive Processes and Neural Representations that Underlie Declarative Memory. *Neuron*, 44(1):109–120, September 2004. ISSN 0896-6273. doi: 10.1016/j.neuron.2004.08.028. URL <https://www.sciencedirect.com/science/article/pii/S089662730400529X>.
- [13] Russell A Epstein, Eva Zita Patai, Joshua B Julian, and Hugo J Spiers. The cognitive map in humans: spatial navigation and beyond. *Nature neuroscience*, 20(11):1504–1513, 2017.
- [14] Lasse Espeholt, Hubert Soyer, Remi Munos, Karen Simonyan, Vlad Mnih, Tom Ward, Yotam Doron, Vlad Firoiu, Tim Harley, Iain Dunning, et al. Impala: Scalable distributed deep-rl with importance weighted actor-learner architectures. In *International conference on machine learning*, pages 1407–1416. PMLR, 2018.

- [15] Dave Ferguson, Maxim Likhachev, and Anthony Stentz. A guide to heuristic-based path planning. In *Proceedings of the international workshop on planning under uncertainty for autonomous systems, international conference on automated planning and scheduling (ICAPS)*, pages 9–18, 2005.
- [16] James Gornet and Matt Thomson. Automated construction of cognitive maps with visual predictive coding. *Nature Machine Intelligence*, 6(7):820–833, 2024.
- [17] Albert Gu and Tri Dao. Mamba: Linear-time sequence modeling with selective state spaces, 2024. URL <https://arxiv.org/abs/2312.00752>.
- [18] Agrim Gupta, Stephen Tian, Yunzhi Zhang, Jiajun Wu, Roberto Martín-Martín, and Li Fei-Fei. Maskvit: Masked visual pre-training for video prediction. *arXiv preprint arXiv:2206.11894*, 2022.
- [19] David Ha and Jürgen Schmidhuber. World models. *arXiv preprint arXiv:1803.10122*, 2018.
- [20] Danijar Hafner, Timothy Lillicrap, Jimmy Ba, and Mohammad Norouzi. Dream to control: Learning behaviors by latent imagination. *arXiv preprint arXiv:1912.01603*, 2019.
- [21] Danijar Hafner, Timothy Lillicrap, Mohammad Norouzi, and Jimmy Ba. Mastering atari with discrete world models. *arXiv preprint arXiv:2010.02193*, 2020.
- [22] Danijar Hafner, Jurgis Pasukonis, Jimmy Ba, and Timothy Lillicrap. Mastering diverse domains through world models. *arXiv preprint arXiv:2301.04104*, 2023.
- [23] Torkel Hafting, Marianne Fyhn, Sturla Molden, May-Britt Moser, and Edvard I. Moser. Microstructure of a spatial map in the entorhinal cortex. *Nature*, 436(7052):801–806, August 2005. ISSN 1476-4687. doi: 10.1038/nature03721. URL <https://www.nature.com/articles/nature03721>. Number: 7052 Publisher: Nature Publishing Group.
- [24] Peter E Hart, Nils J Nilsson, and Bertram Raphael. A formal basis for the heuristic determination of minimum cost paths. *IEEE transactions on Systems Science and Cybernetics*, 4(2):100–107, 1968.
- [25] D. Hassabis, D. Kumaran, S. D. Vann, and E. A. Maguire. Patients with hippocampal amnesia cannot imagine new experiences. *Proceedings of the National Academy of Sciences*, 104(5): 1726–1731, 2007. ISSN 0027-8424. doi: 10.1073/pnas.0610561104. URL <http://www.pnas.org/cgi/doi/10.1073/pnas.0610561104>. Number: 5.
- [26] Sepp Hochreiter and Jürgen Schmidhuber. Long Short-Term Memory. *Neural Computation*, 9(8):1735–1780, November 1997. ISSN 0899-7667. doi: 10.1162/neco.1997.9.8.1735. Conference Name: Neural Computation.
- [27] Marc W. Howard and Howard Eichenbaum. Time and space in the hippocampus. *Brain Research*, 1621:345–354, September 2015. ISSN 0006-8993. doi: 10.1016/j.brainres.2014.10.069. URL <https://www.sciencedirect.com/science/article/pii/S0006899314014917>.
- [28] Lukasz Kaiser, Mohammad Babaeizadeh, Piotr Milos, Blazej Osinski, Roy H Campbell, Konrad Czechowski, Dumitru Erhan, Chelsea Finn, Piotr Kozakowski, Sergey Levine, et al. Model-based reinforcement learning for atari. *arXiv preprint arXiv:1903.00374*, 2019.
- [29] Pentti Kanerva. *Sparse distributed memory*. MIT press, 1988.
- [30] Arbaaz Khan, Clark Zhang, Nikolay Atanasov, Konstantinos Karydis, Vijay Kumar, and Daniel D. Lee. Memory Augmented Control Networks, February 2018. URL <http://arxiv.org/abs/1709.05706>. arXiv:1709.05706 [cs].
- [31] Apoorv Khandelwal, Luca Weihs, Roozbeh Mottaghi, and Aniruddha Kembhavi. Simple but effective: Clip embeddings for embodied ai. In *Proceedings of the IEEE/CVF Conference on Computer Vision and Pattern Recognition*, pages 14829–14838, 2022.
- [32] Daniel P. Kimble. The effects of bilateral hippocampal lesions in rats. *Journal of Comparative and Physiological Psychology*, 56(2):273–283, 1963. ISSN 0021-9940. doi: 10.1037/h0048903. URL <https://doi.apa.org/doi/10.1037/h0048903>.

- [33] Christopher J. Kymn, Sonia Mazelet, Anthony Thomas, Denis Kleyko, E. P. Frady, Friedrich T. Sommer, and Bruno A. Olshausen. Binding in hippocampal-entorhinal circuits enables compositionality in cognitive maps. *Advances in Neural Information Processing Systems*, 37:39128–39157, December 2024. URL https://proceedings.neurips.cc/paper_files/paper/2024/hash/4526cfacdbca6b6e184568dac91bf070-Abstract-Conference.html.
- [34] Daniel Levenstein, Aleksei Efremov, Roy Henha Eyono, Adrien Peyrache, and Blake A. Richards. Sequential predictive learning is a unifying theory for hippocampal representation and replay, April 2024. URL <https://www.biorxiv.org/content/10.1101/2024.04.28.591528v1>. Pages: 2024.04.28.591528 Section: New Results.
- [35] Sam McKenzie, Andrea J. Frank, Nathaniel R. Kinsky, Blake Porter, Pamela D. Rivière, and Howard Eichenbaum. Hippocampal Representation of Related and Opposing Memories Develop within Distinct, Hierarchically Organized Neural Schemas. *Neuron*, 83(1):202–215, July 2014. ISSN 0896-6273. doi: 10.1016/j.neuron.2014.05.019. URL [https://www.cell.com/neuron/abstract/S0896-6273\(14\)00405-X](https://www.cell.com/neuron/abstract/S0896-6273(14)00405-X). Publisher: Elsevier.
- [36] Vincent Micheli, Eloi Alonso, and François Fleuret. Transformers are sample-efficient world models. *arXiv preprint arXiv:2209.00588*, 2022.
- [37] Volodymyr Mnih. Asynchronous methods for deep reinforcement learning. *arXiv preprint arXiv:1602.01783*, 2016.
- [38] Shinya Nakai, Takuma Kitanishi, and Kenji Mizuseki. Distinct manifold encoding of navigational information in the subiculum and hippocampus. *Science Advances*, 10(5):ead14471, 2024. doi: 10.1126/sciadv.adi4471. URL <https://www.science.org/doi/abs/10.1126/sciadv.adi4471>.
- [39] John O’Keefe. Place units in the hippocampus of the freely moving rat. *Experimental Neurology*, 51(1):78–109, January 1976. ISSN 0014-4886. doi: 10.1016/0014-4886(76)90055-8. URL <https://www.sciencedirect.com/science/article/pii/0014488676900558>.
- [40] John O’Keefe and Lynn Nadel. *The hippocampus as a cognitive map*. Oxford: Clarendon Press, 1978.
- [41] Scott Reed, Konrad Zolna, Emilio Parisotto, Sergio Gomez Colmenarejo, Alexander Novikov, Gabriel Barth-Maron, Mai Gimenez, Yury Sulsky, Jackie Kay, Jost Tobias Springenberg, et al. A generalist agent. *arXiv preprint arXiv:2205.06175*, 2022.
- [42] Sam Ritter, Ryan Faulkner, Laurent Sartran, Adam Santoro, Matt Botvinick, and David Raposo. Rapid task-solving in novel environments. *arXiv preprint arXiv:2006.03662*, 2020.
- [43] Jan Robine, Marc Höftmann, Tobias Uelwer, and Stefan Harmeling. Transformer-based world models are happy with 100k interactions. *arXiv preprint arXiv:2303.07109*, 2023.
- [44] Julian Schrittwieser, Ioannis Antonoglou, Thomas Hubert, Karen Simonyan, Laurent Sifre, Simon Schmitt, Arthur Guez, Edward Lockhart, Demis Hassabis, Thore Graepel, et al. Mastering atari, go, chess and shogi by planning with a learned model. *Nature*, 588(7839):604–609, 2020.
- [45] W. B. Scoville and B. Milner. Loss of recent memory after bilateral hippocampal lesions. *Journal of neurology, neurosurgery, and psychiatry*, 20(1):11–21, 1957. ISSN 00223050. doi: 10.1136/jnnp.20.1.11. Number: 1.
- [46] Dhruv Shah, Ajay Sridhar, Nitish Dashora, Kyle Stachowicz, Kevin Black, Noriaki Hirose, and Sergey Levine. ViNT: A Foundation Model for Visual Navigation, June 2023. URL <http://arxiv.org/abs/2306.14846>. arXiv:2306.14846 [cs].
- [47] Kimberly L. Stachenfeld, Matthew M. Botvinick, and Samuel J. Gershman. The hippocampus as a predictive map. *Nature Neuroscience*, 20(11):1643–1653, 2017. ISSN 15461726. doi: 10.1038/nn.4650. URL <http://dx.doi.org/10.1038/nn.4650>. Number: 11 arXiv: 1011.1669v3 Publisher: Nature Publishing Group ISBN: 9788578110796.
- [48] Richard S Sutton. Reinforcement learning: An introduction. *A Bradford Book*, 2018.

- [49] Joshua B Tenenbaum, Vin de Silva, and John C Langford. A global geometric framework for nonlinear dimensionality reduction. *science*, 290(5500):2319–2323, 2000.
- [50] Thomas Unterthiner, Sjoerd Van Steenkiste, Karol Kurach, Raphael Marinier, Marcin Michalski, and Sylvain Gelly. Towards accurate generative models of video: A new metric & challenges. *arXiv preprint arXiv:1812.01717*, 2018.
- [51] Ashish Vaswani, Noam Shazeer, Niki Parmar, Jakob Uszkoreit, Llion Jones, Aidan N. Gomez, Lukasz Kaiser, and Illia Polosukhin. Attention Is All You Need, December 2017. URL <http://arxiv.org/abs/1706.03762>. arXiv:1706.03762 [cs].
- [52] Raymond Wang, Jaedong Hwang, Akhilan Boopathy, and Ila R. Fiete. Rapid Learning without Catastrophic Forgetting in the Morris Water Maze. 2023. URL <https://openreview.net/forum?id=MUANyzcyrS>.
- [53] Manuel Watter, Jost Springenberg, Joschka Boedecker, and Martin Riedmiller. Embed to control: A locally linear latent dynamics model for control from raw images. *Advances in neural information processing systems*, 28, 2015.
- [54] James C. R. Whittington, Timothy H. Muller, Shirley Mark, Guifen Chen, Caswell Barry, Neil Burgess, and Timothy E. J. Behrens. The Tolman-Eichenbaum Machine: Unifying Space and Relational Memory through Generalization in the Hippocampal Formation. *Cell*, 183(5):1249–1263.e23, November 2020. ISSN 0092-8674, 1097-4172. doi: 10.1016/j.cell.2020.10.024. URL [https://www.cell.com/cell/abstract/S0092-8674\(20\)31388-X](https://www.cell.com/cell/abstract/S0092-8674(20)31388-X). Publisher: Elsevier.
- [55] James C. R. Whittington, Joseph Warren, and Timothy E. J. Behrens. Relating transformers to models and neural representations of the hippocampal formation, 2022. URL <http://arxiv.org/abs/2112.04035>. arXiv:2112.04035 [cs, q-bio].
- [56] James CR Whittington, David McCaffary, Jacob JW Bakermans, and Timothy EJ Behrens. How to build a cognitive map. *Nature neuroscience*, 25(10):1257–1272, 2022.
- [57] Erik Wijmans, Abhishek Kadian, Ari Morcos, Stefan Lee, Irfan Essa, Devi Parikh, Manolis Savva, and Dhruv Batra. Dd-ppo: Learning near-perfect pointgoal navigators from 2.5 billion frames. *arXiv preprint arXiv:1911.00357*, 2019.
- [58] Erik Wijmans, Manolis Savva, Irfan Essa, Stefan Lee, Ari S Morcos, and Dhruv Batra. Emergence of maps in the memories of blind navigation agents. *AI Matters*, 9(2):8–14, 2023.
- [59] Matthew A. Wilson and Bruce L. McNaughton. Dynamics of the Hippocampal Ensemble Code for Space. *Science*, 261(5124):1055–1058, August 1993. doi: 10.1126/science.8351520. URL <https://www.science.org/doi/abs/10.1126/science.8351520>. Publisher: American Association for the Advancement of Science.
- [60] Brian Yamauchi. A frontier-based approach for autonomous exploration. In *Proceedings 1997 IEEE International Symposium on Computational Intelligence in Robotics and Automation CIRA'97. Towards New Computational Principles for Robotics and Automation*, pages 146–151. IEEE, 1997.
- [61] Weipu Zhang, Gang Wang, Jian Sun, Yetian Yuan, and Gao Huang. Storm: Efficient stochastic transformer based world models for reinforcement learning. *Advances in Neural Information Processing Systems*, 36, 2024.

A Extended Methods

A.1 Training Details

Transition Embedding. In the `Open Arena` environment, each state value is encoded as a 6-bit binary. Each bit is independently projected—via either the source-state or end-state linear projector—into a 128-dimensional embedding. The six embeddings are concatenated into a single 768-dimensional state vector. Actions are similarly mapped into 768-dimensional embeddings using a dedicated linear projector. The final transition embedding is then obtained by averaging the three 768-dimensional vectors corresponding to (1) the start-state, (2) the action, and (3) the end-state.

In the `Random Wall` environment, the same procedure applies, except that each state is represented by an integer and projected into a 1,024-dimensional embedding, yielding a 1,024-dimensional transition vector.

Model Architectures.

- **Transformer:** 8 attention heads per layer; feed-forward hidden dimension of 2,048.
- **LSTM:** hidden state size of 1,024.
- **Mamba:** model dimension of 768 in `Open Arena` and 1,024 in `Random Wall`.

Training Hyperparameters. All models were trained on a single NVIDIA A100 GPU for 480,000 iterations using:

- Optimizer: AdamW with initial learning rate 1×10^{-4} and cosine decay schedule.
- Dropout: 0.1.
- Batch size: 128 memory bank and query pairs.
- Training time: 19–28 hours, depending on model capacity.
- Memory usage: 2GB. The low memory consumption is attributed to the online generation of data.

A.2 Building Random Environments

To generate an input (memory bank, query) pair to ESWM, we first generate an environment $e \in \mathcal{E}$. Each e is represented as a 5-tuple (G, g, W, ψ, A) , where:

- $G = (L, E)$: An undirected graph, with L representing unique locations and E representing undirected edges connecting adjacent locations. The graph G adopts a fixed hexagonal structure across all environments. It models grid-like movement dynamics and serves as the canvas for creating complex environments.
- g : A filtering function that generates a subgraph $G_{\text{obs}} \subseteq G$, containing only observable locations $L_{\text{obs}} \subseteq L$ and transitions $E_{\text{obs}} \subseteq E$ (i.e. part of the environment that will be observable to the agent in that sample).
- W : A subset of contiguous locations in L , representing a wall that restrict agent’s motion in the environment.
- ψ : A mapping from L to integer observations, assigning each location to a unique observation from $S \subseteq \mathbb{Z}$. This allows random association of locations and observed values (or states) in each sample.
- A : Maps an undirected edge $e = (l_i, l_j) \in E$, which is a pair of locations, to an action-induced transition either starting from l_i or l_j with equal chances. e.g. $A(l_i, l_j)$ returns a 3-tuple transition $(l_i, \text{go West}, l_j)$ or $(l_j, \text{go East}, l_i)$ with equal probability.

In the `Open Arena` setting (Section 3.3), the entire environment is observable and there are no obstacles (i.e. g is the identity function, $W = \emptyset$). In the `Random Wall` setting (Section 3.3), g removes a random subset $V_{\text{unobs}} \subseteq V$ along with their attached edges, and $W \neq \emptyset$. The components g , W , and ψ are randomly generated for each environment e , where applicable.

A.3 Generating Memory Banks

The minimal spanning episodic memories M for an environment $e = (G, g, W, \psi, A)$ is generated as follows:

1. Apply the filtering function g to G to produce the partially observed subgraph $G_{\text{obs}} = (L_{\text{obs}}, E_{\text{obs}})$.
2. Run a minimal spanning tree (MST) algorithm on G_{obs} , with random weights assigned to edges to ensure diversity. Tree effectively models a set of fragmented transitions that do not naturally integrate into a continuous trajectory. This produces a set of undirected edges $T = \{(l_i, l_j) \mid l_i, l_j \in L_{\text{obs}}\}$.
3. Use A to map edges in T to directed 3-tuple transitions between locations and ψ to map locations to observations. This produces an array of transitions between observations $[(s_s, a, s_e)]$.
4. Modify transitions ending at locations in W to form self-loops, effectively modeling blocked movement. Then, randomly permute the array of transitions to produce the final array of transitions M .

In `Open Arena` and `Random Wall`, the memory banks M observe at most 18 and 36 transitions out of the total 84 and 180 transitions, respectively.

A.4 Query Selection

The resulting memory bank M is an unordered set of one-step transitional episodic memories that span all observable locations in the environment (Fig.2). Given M , the model is tasked to infer the missing component of a query transition $q = (s_s, a, s_e)$.

For `Random Wall`, the query q is selected from 1) the set of transitions that are in G_{obs} but not in the memory bank (unseen transitions; 68%); 2) from the memory bank (seen transitions; 15%) and; 3) from a set of unsolvable transitions where one end is in L_{unobs} (17%). In `Open Arena`, the query q is always selected from unseen transitions.

The model receives the M and $q = (s_s, a, s_e)$, with either s_s , a , or s_e masked randomly with equal probability, as input, and asked to infer the masked compartment.

A.5 ISOMAP

We consider ESWM’s population neuron activity at a particular location as the ESWM’s activation vector as it infers the missing component of a query transition that either starts or ends at that location. For end-state and action predictions (i.e, source state is visible to ESWM), the activation vector is associated with the source state’s location, while for start-state prediction (i.e, source state is not visible), we associate the activation with the end state’s location. For transformer models, we used the query token after each transformer encoder block as the activation vector, while for multilayer LSTM and Mamba, we used the final hidden state (i.e, the last token from the processed sequence) from the last layer.

To collect ESWM’s activation across all locations in an environment, we task ESWM to do either start-state, action, or end-state prediction for all transitions in the environment conditioned on a memory bank. This process is repeated with multiple memory banks from the same environment until approximately 1,000 activation vectors are collected. We then apply ISOMAP using cosine distance and 20–60 neighbors to generate the visualizations.

A.6 Euclidean Distance Estimation From Activation

A linear layer receives as input the concatenation of three vectors: the activations from Transformer-2L ESWM corresponding to action predictions starting from states A, B, and C. It outputs a scalar representing the probability that the Euclidean distance between A and B exceeds that between A and C. The classifier is trained on 3,000 state triplets sampled all from different environments and evaluated on 1,000 held-out triplets. Reported accuracies are averaged over 10 runs with different randomly initialized weights for the linear layer.

A.7 Baseline Navigational Agent

The baseline agent is trained via A2C (48; 37) to navigate between any two states in a single Random Wall environment, which differs from ESWM and EPN, which are meta-trained across many environments. At each time step t , the agent receives as input a sequence of historical interactions with the environment, each as a tuple $(s_{t-1}, a_{t-1}, s_t, s_{\text{goal}})$, and is tasked to output an action towards the goal state s_{goal} . Each part of the tuple is distinctly embedded onto a 128D vector and the vectors are averaged to produce the final observation at each time step. The embedded sequence is fed into a one-layer LSTM (with a hidden dimension of 256) and the predicted action and value are read out from the final hidden state via distinct linear heads.

The agent receives a penalty of -0.01 every time step except when it reaches the goal state, where it receives a reward of 1. The training is done over 5000 episodes with a discount factor of 0.99 and learning rate of 1×10^{-3} .

B Additional Figures

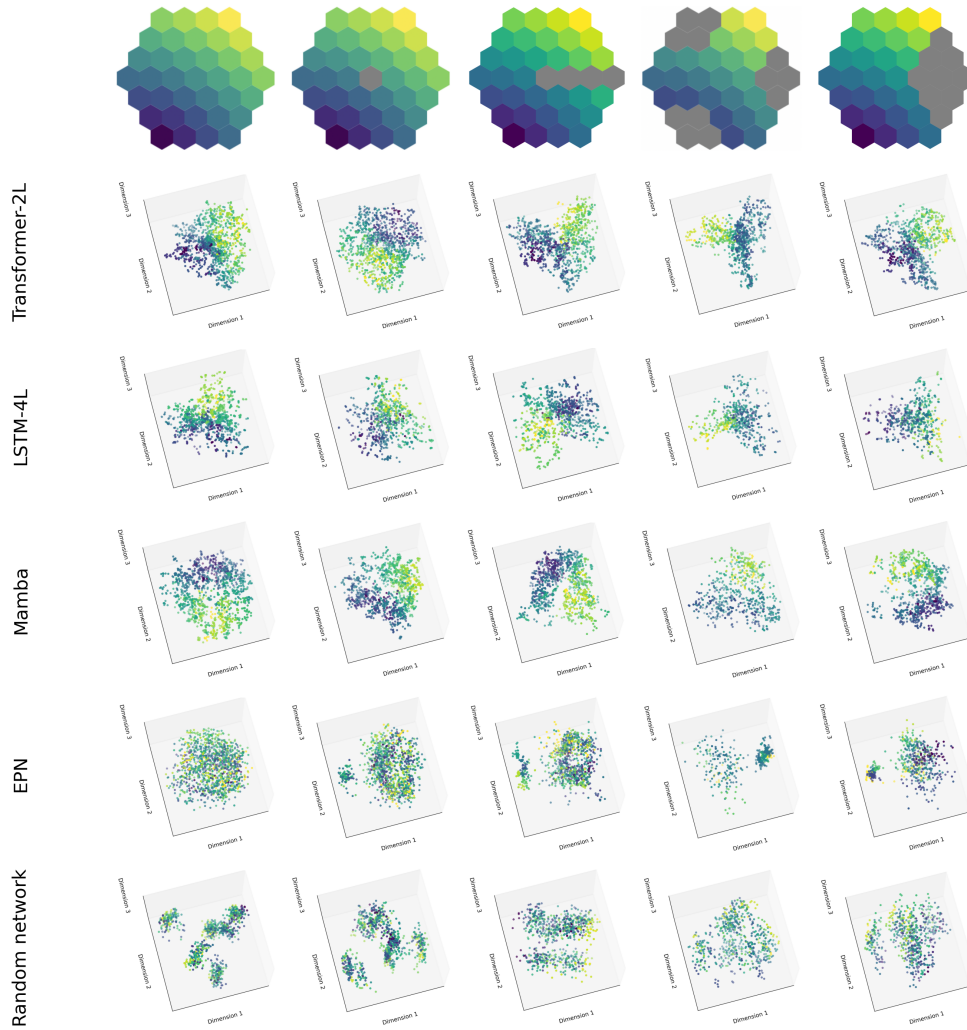


Figure A1: **ISOMAP projection of various ESWM-trained models' latent space.** The last two environments are **out-of-distribution** — ESWM has never seen multiple walls in the same room nor a cluster of obstacles that does not form a long, straight wall during training. For Transformer-2L, LSTM-4L, and Random network (LSTM-4L initialized with random weights), the activations for end-state prediction are used while for Mamba, the activations for action prediction are used. EPN (Section D) is an episodic-memory-based navigational and exploration agent trained on the same environment as ESWM.

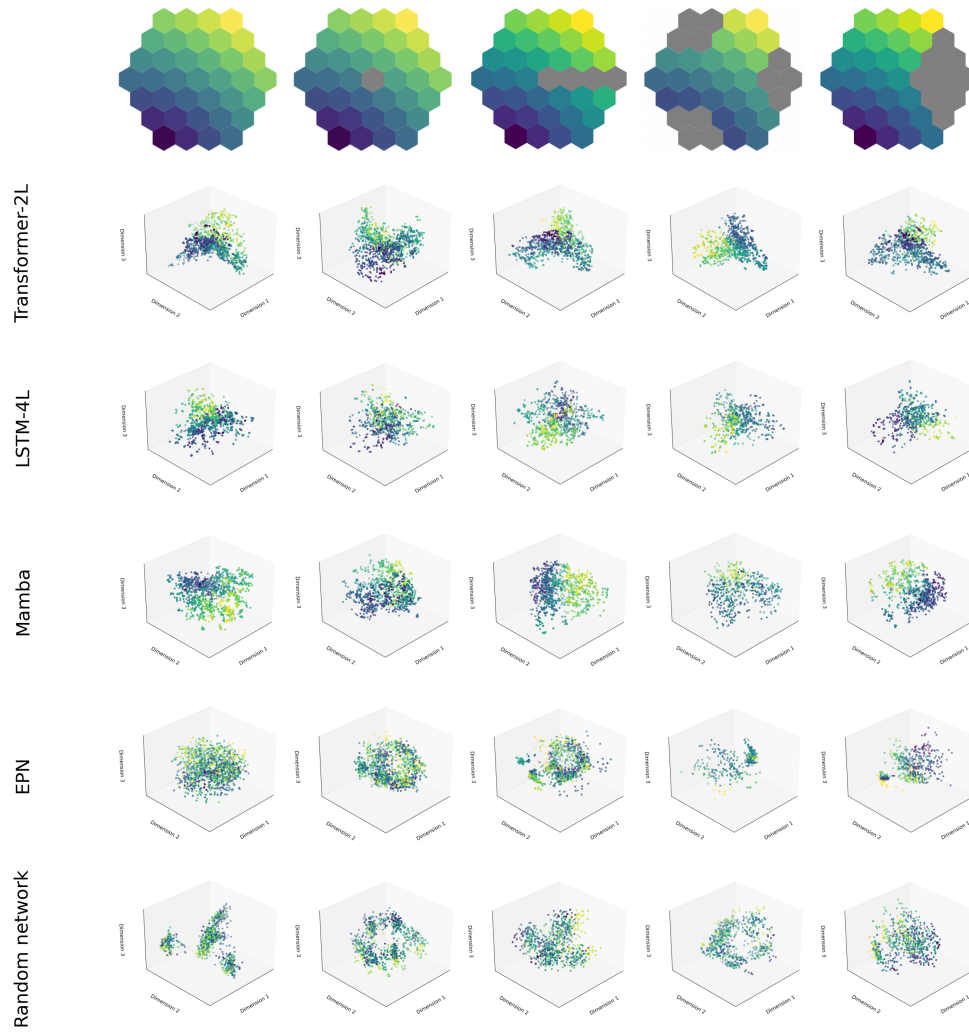


Figure A2: Same ISOMAP projections as Fig.A1 but in a different angle.

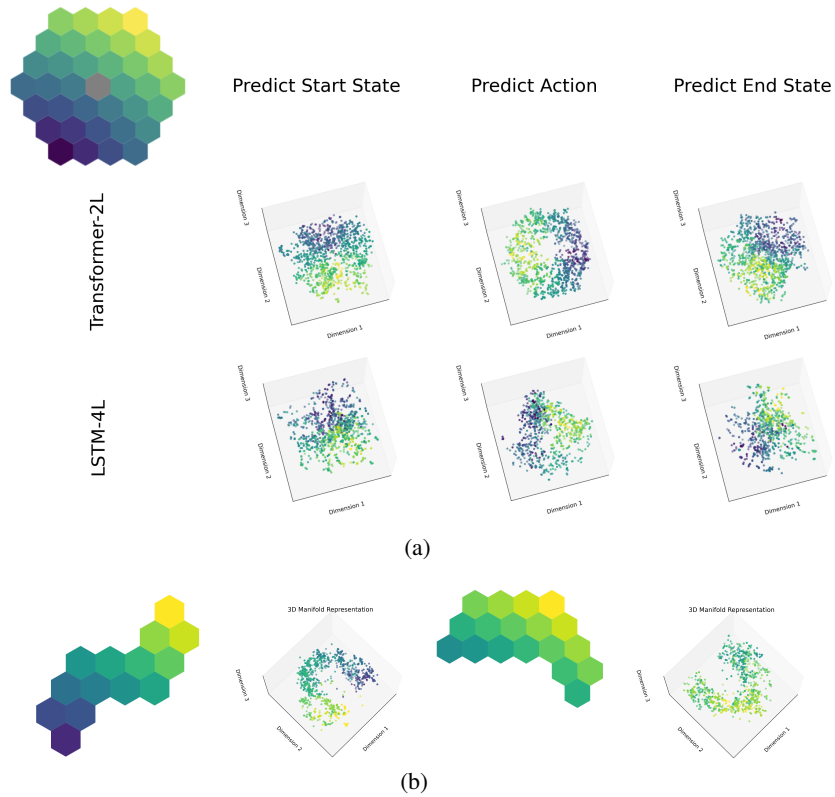


Figure A3: **ESWM's latent spatial map persists for all prediction tasks and partial observations.** **a)** ESWM's latent spatial map for start-state, action, and end-state predictions. Mamba is excluded as the spatial map is only found for the action prediction task. For Transformer-2L, the spatial map is found in the first layer for action prediction, and the second layer for start-state and end-state prediction. **b)** Spatial map when the memory bank observes an irregular subsection of the room. Transformer-2L's first layer's activation for action prediction is used.

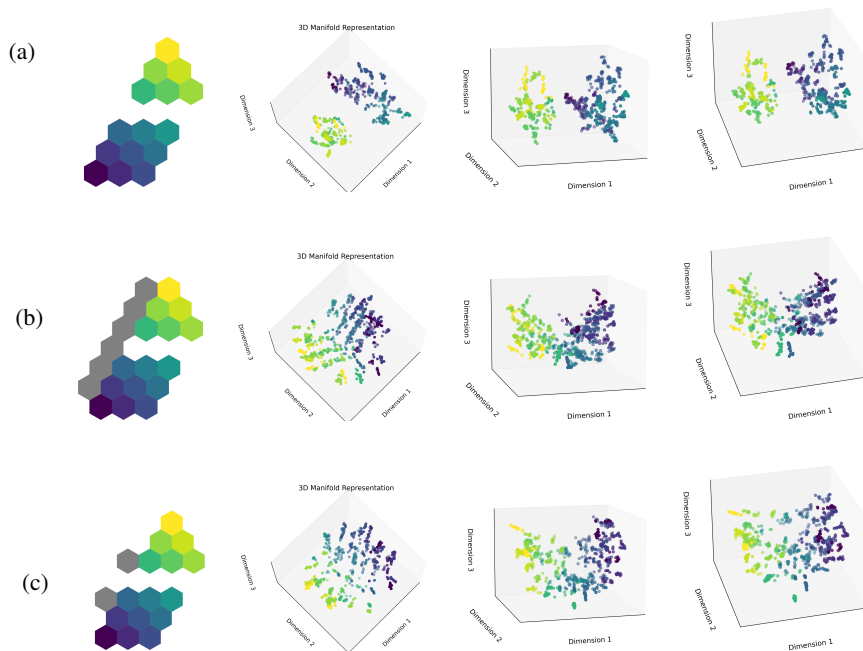


Figure A4: **ESWM's latent spatial map adjusts to structural changes.** ISOMAP projections of the 14-layer transformer model's seventh layer's activations. **a)** ESWM's latent space when the input memory bank M consists of two disjoint memory clusters. **b)** ESWM's latent space when both memory clusters observe a wall to their left; despite remaining separate in the memory bank, ESWM inferred them to be connected as reflected in its latent space. **c)** ESWM's latent space when both memory clusters observe a single obstacle to their left. ESWM, again, inferred the clusters are connected but with sparser observations of obstacles than in b). 900 activations and 45 neighbours are used to fit the ISOMAP.

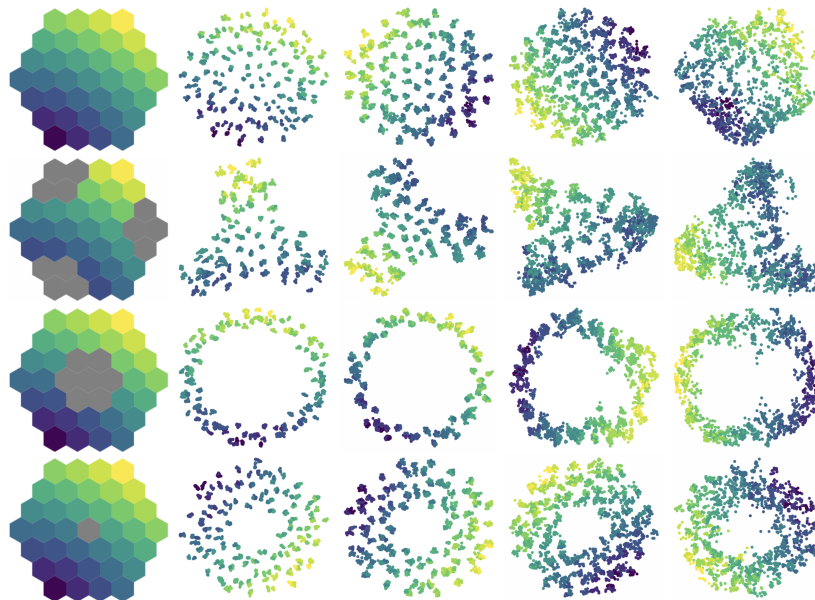


Figure A5: **Representation becomes more continuous with depth.** Left to right are 30-neighbours ISOMAP projections from layer 1, 6, 9, and 14 of Transformer-14L (2000 activations). The model was trained without random masking of subregions. Representation in the latent space becomes progressively more continuous.

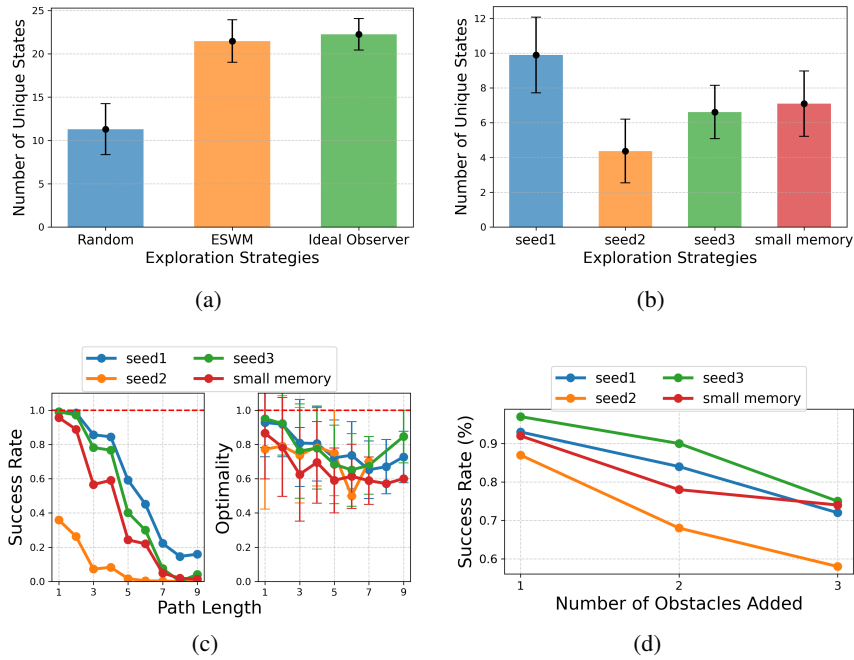


Figure A6: **Exploration, navigation, and adaptability for ESWM and EPN.** **a)** Number of unique states visited by different exploration strategies in a Random Wall environment with 37 locations over 25 time steps ($n=1000$). On average, ESWM explores a comparable number of states to an oracle explorer with access to obstacle locations. **b, c, d)** Performance on Random Wall with 19 locations of individual EPN's random seeds, and EPN with memory bank size ablated from 200 to 50 (small memory). **b)** Number of unique states visited over the initial 15 time steps in a novel environment. **c)** Navigation success rate and optimality when tasked to navigate to a goal across various path lengths, $n = 2400$ paths. **d)** Adaptation to structural changes in the environment. Success rate of navigating to a goal location when obstacles contradicting past experiences are inserted

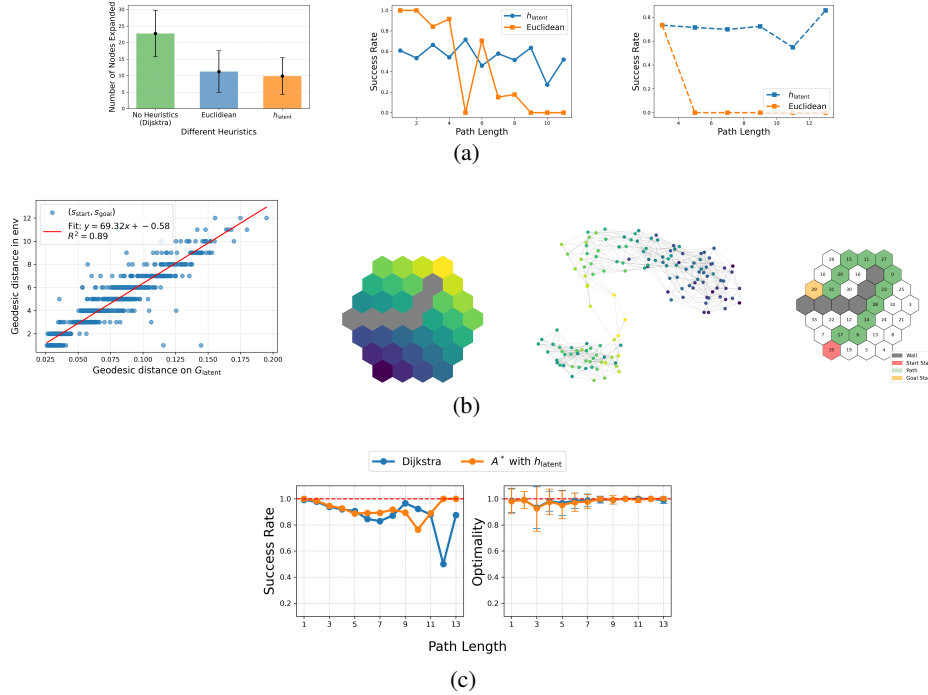


Figure A7: **The latent space of ESWM can be harnessed as a heuristic for more efficient planning.** All the results are on Random Wall environment with 37 locations. **a)** (Left) Average number of nodes expanded for different heuristics over 1000 paths. (Middle) Success rates of greedy navigation using different heuristics over 2400 paths. (Right) Success rates for greedy navigation on paths requiring detours around obstacles over 800 paths. **b)** (Left) Correlation between geodesic distances on G_{latent} (see 4.6.2) and corresponding distances in the environment, using $n=1500$ pairs of states ($s_{\text{start}}, s_{\text{goal}}$) over 75 environments. The linear fit shows a strong positive correlation with $R^2 = 0.89$. (Mid-Left) sample grid environment. (Mid-Right) G_{latent} for the same environment. (Right) Agent navigates greedily on h_{latent} on a path that requires detours around obstacles. **c)** Comparison of navigation success rate and path optimality between Dijkstra's and A* over different path lengths ($n=1500$). Although not guaranteed to be admissible, h_{latent} empirically preserves path optimality.

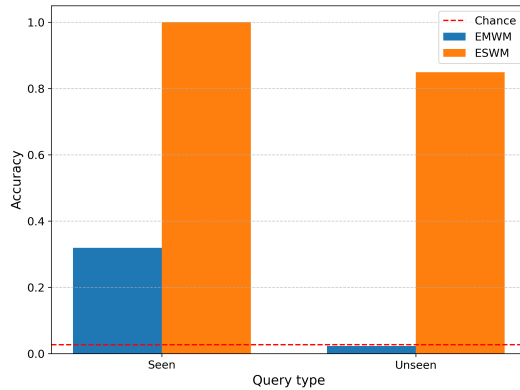


Figure A8: **Comparison of end-state prediction accuracy between EMWM (8) and Transformer-2L ESWM in RandomWall.** EMWM predicts using a weighted average over the top-K matches ($K=5$), but we found $K=1$ performs best, likely due to the sparsity of our memory banks (i.e., transitions are unique, so averaging more than one transition offers no benefit). To adapt the author’s implementation to our task, we embed each token (transitional memory tokens or the end-state masked query) by averaging the embedding of each item (s_t, a_t, s_{t+1}), each produced using a distinct MLP layer – identical to ESWM. All tokens are sequentially fed into a 1-layer GRU (7) to obtain the sequence of hidden states, which become the keys with the corresponding end-state embeddings as values for the memory table. The network is optimized to predict the s_{t+1} for each token.

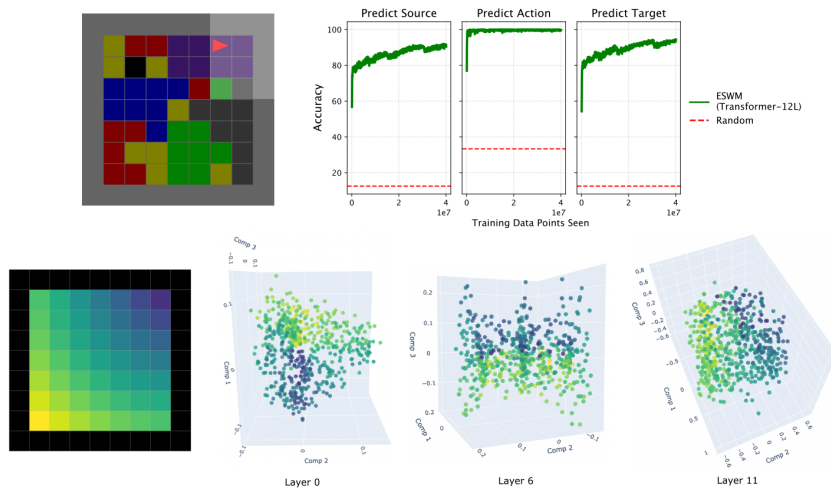


Figure A9: **ESWM in scaled-up MiniGrid environments.** (Top left) An example of a procedurally-generated 9×9 environment with random coloring patterns in which ESWM is trained. Episodic memory is considered as a transition between 5×5 egocentric pixel observations via egocentric actions (turn left, turn right, and move forward). Memory bank is a set of one-step transitions that minimally observe the entire room, with some degree of overlap between transitions to enable memory integration. (Top right) Accuracies for start-state, action, and end-state predictions. (Bottom) ISOMAP analysis on ESWM’s latent space shows a map-like representation.

C Algorithms

Algorithm 1 Dijkstra-Style Pathfinding with ESWM

```

1: procedure FINDPATH(ESWM, memoryBank,  $s_{\text{start}}$ ,  $s_{\text{goal}}$ ,  $T_{\text{max}}$ )
2:   const ACTION_COST
3:   Initialize priority queue OpenSet
4:   Initialize dictionary Cost
5:   Initialize dictionary Parent
6:    $Cost[s_{\text{start}}] = 0$ ,  $Parent[s_{\text{start}}] = \text{nil}$ 
7:   Push ( $s_{\text{start}}$ ,  $cost = 0$ ,  $depth = 0$ ) into OpenSet
8:   while OpenSet  $\neq \emptyset$  do
9:     ( $u$ ,  $c$ ,  $d$ )  $\leftarrow$  PopMinCostNode(OpenSet)
10:    if  $u = s_{\text{goal}}$  then
11:      return ReconstructPath(Parent,  $u$ )
12:    end if
13:    if  $d \geq T_{\text{max}}$  then
14:      continue  $\triangleright$  remove path that exceeds horizon
15:    end if
16:    for all action  $a$  in PossibleActions do
17:       $v \leftarrow$  PredictNextState(ESWM, memoryBank,  $u$ ,  $a$ )
18:       $c' \leftarrow c + ACTION\_COST$ 
19:       $d' \leftarrow d + 1$ 
20:      if  $v$  not in Cost or  $c' < Cost[v]$  then
21:        Push ( $v$ ,  $c'$ ,  $d'$ ) into OpenSet
22:         $Cost[v] = c'$ 
23:         $Parent[v] = u$ 
24:      end if
25:    end for
26:  end while
27:  return FAIL()  $\triangleright$  no path within horizon  $T_{\text{max}}$ 
28: end procedure

```

Algorithm 2 Explore Function

```

1: procedure EXPLORE(ESWM, memoryBank,  $s$ , actions)  $\triangleright$   $s$  is current observation
2:   Initialize  $q$  as a max heap
3:   for all  $a \in$  actions do
4:      $s'$ , logits  $\leftarrow$  ESWM.PREDICTEND(memoryBank,  $s$ ,  $a$ )
5:     probs  $\leftarrow$  SOFTMAX(logits)
6:     if  $s' =$  'I don't know' then
7:       Enqueue  $a$  into  $q$  with cost =  $1 - \beta \text{ENTROPY}(\text{probs})$   $\triangleright$   $\beta = 0.2$  in our experiments
8:     else if  $\text{probs}[s'] \leq 0.8$  then
9:       Enqueue  $a$  into  $q$  with cost =  $\gamma \text{ENTROPY}(\text{probs})$   $\triangleright$   $\gamma = 0.1$  in our experiments
10:    end if
11:  end for
12:  return  $q$ .REMOVEMAX()
13: end procedure

```

Algorithm 3 Get all State-Action Pairs

```
1: procedure GETSAS(memoryBank)
2:    $S \leftarrow \text{GETUNIQUESTATES}(\text{memoryBank})$ 
3:   Initialize  $l$  as an empty list
4:   for all  $s \in S$  do
5:     for all  $a \in \text{Actions}$  do
6:        $l.append((s, a))$ 
7:     end for
8:   end for
9:   return  $l$ 
10: end procedure
```

Algorithm 4 Compute Geodesic Distance Table h_{latent}

```
1: procedure GETHEURISTICS(ESWM, memoryBank,  $R_{\text{latent}}$ )
2:    $SAs \leftarrow \text{GETSAS}(\text{memoryBank})$ 
3:    $N \leftarrow |SAs|$ 
4:   Initialize  $nodesToSAs$  as an empty dictionary
5:   Initialize  $activations$  as an empty list
6:   Initialize  $h_{\text{latent}}$  as a matrix of shape  $N \times N$ 
7:   for all  $(s, a) \in saPairs$  do
8:      $activation \leftarrow \text{ESWM's activation for end state prediction task starting at } s \text{ taking action } a$ 
9:      $nodesToSAs[activation] \leftarrow (s, a)$ 
10:     $activations.append(activation)$ 
11:  end for
12:   $G_{\text{latent}} \leftarrow \text{NEARESTNEIGHBOURGRAPH}(activations, R_{\text{latent}})$ 
13:  for all  $n_i \in G_{\text{latent}}.nodes$  do
14:    for all  $n_j \in G_{\text{latent}}.nodes$  do  $\triangleright n_i, n_j$  are activations
15:       $sa_i, sa_j \leftarrow nodesToSAs[n_i], nodesToSAs[n_j]$ 
16:       $h_{\text{latent}}[sa_i, sa_j] \leftarrow \text{SHORTESTPATHLENGTH}(G_{\text{latent}}, n_i, n_j)$ 
17:    end for
18:  end for
19:  return  $h_{\text{latent}}$ 
20: end procedure
```

Note that h_{latent} approximates the geodesic distance between any two state-action pairs rather than between any two states. Geodesic distances between states can be obtained by averaging over the action space.

Selection of R_{latent}

In essence, R_{latent} is the radius among a set of radii R in which the corresponding h_{latent} , obtained from Alg.4, best captures the geodesic distance information in the environment. More specifically, R_{latent} is the $r \in R$ that maximizes both the success rate and the optimality of the agent's path when it navigates greedily to the corresponding h_{latent} . We consider a navigation as successful if the agent reaches the goal state within 20 time steps. Path optimality is measured by the ratio between the shortest path and the agent's path. To determine R_{latent} , we conducted a search over a bounded range R , which includes those whose ISOMAP projections accurately reflect the structure of the environment.

Limitations of Alg4

One drawback is that h_{latent} can overestimate the true geodesic distance, i.e. it is non-admissible. This is because G_{latent} might be under-connected for the given R_{latent} and memory bank (i.e. nodes aren't connected by an edge when they should). This can be mitigated by using a larger radius $R_{\text{latent}} + \epsilon$ to build G_{latent} (i.e. prefer over-connection over under-connection). However, we acknowledge that there is no way to guarantee admissibility, hence, the optimality of the path. This is a trade-off for

faster search. In future work, we will explore adaptive radius where radius, hence h_{latent} , can be adjusted dynamically as agents interact with the environment.

D Episodic Planning Networks (EPN)

The Episodic Planning Networks (EPN) model (42) is specifically designed and trained to rapidly learn to navigate in novel environments. Comparatively, ESWM is a general-purpose model not explicitly trained for navigation. By comparing with EPN, we investigate whether ESWM’s ability to construct internal models of spatial structures enables navigational capabilities. Similarly to ESWM, EPN is designed to leverage episodic memory to facilitate rapid adaptation in unfamiliar environments, and both models are episodic memory-driven transformer-based models.

Hyperparameters – We use the same hyperparameters as those reported by Ritter et al. (42).

Training – Both models are trained on the same environment structure variations and amount of data, approximately $1.14e9$ steps, which is a restrictive data regime for EPN. EPN is trained to navigate through reinforcement learning, using IMPALA (14). ESWM is trained to build internal model of environments from sparse disjointed episodic experiences through self-supervision.

Memory bank – EPN has a memory bank containing 200 transitions, whereas ESWM only stores the minimal spanning tree, with 19 transitions for smaller environments and 36 for larger ones. When evaluating EPN ability to navigate, we follows the methodology from Ritter et al. (42). EPN explores to populate its memory bank for the first 2/3 of episodes, and the performance is only measured on the last third.

E Impact Statements

This paper presents work whose goal is to advance the field of Machine Learning. There are many potential societal consequences of our work, particularly in autonomous exploration, navigation, and decision-making in real-world environments. While our work primarily focuses on theoretical and methodological advancements, potential societal consequences include enhanced autonomous navigation technologies, more efficient exploration strategies in robotics, and improved AI models inspired by human cognitive abilities. We also acknowledge the potential misuse of the technology in collecting sensitive data and the ethical considerations regarding the deployment of autonomous agents in critical decision-making scenario, emphasizing the importance of responsible and safe integration of such models in real-world applications.